The role of transmembrane channel–like proteins in the operation of hair cell mechanotransducer channels

Kyunghee X. Kim,[1] Maryline Beurg,[1] Carole M. Hackney,[2] David N. Furness,[3] Shanthini Mahendrasingam,[3] and Robert Fettiplace[1]

[1]Department of Neuroscience, University of Wisconsin Medical School, Madison, WI 53706
[2]Department of Biomedical Science, University of Sheffield, Sheffield S10 2TN, England, UK
[3]Institute for Science and Technology in Medicine, School of Life Sciences, Keele University, Keele, Staffs ST5 5BG, England, UK

Sound stimuli elicit movement of the stereocilia that make up the hair bundle of cochlear hair cells, putting tension on the tip links connecting the stereocilia and thereby opening mechanotransducer (MT) channels. Tmc1 and Tmc2, two members of the transmembrane channel–like family, are necessary for mechanotransduction. To assess their precise role, we recorded MT currents elicited by hair bundle deflections in mice with null mutations of Tmc1, Tmc2, or both. During the first postnatal week, we observed a normal MT current in hair cells lacking Tmc1 or Tmc2; however, in the absence of both isoforms, we recorded a large MT current that was phase-shifted 180°, being evoked by displacements of the hair bundle away from its tallest edge rather than toward it as in wild-type hair cells. The anomalous MT current in hair cells lacking Tmc1 and Tmc2 was blocked by FM1-43, dihydrostreptomycin, and extracellular Ca^{2+} at concentrations similar to those that blocked wild type. MT channels in the double knockouts carried Ca^{2+} with a lower permeability than wild-type or single mutants. The MT current in double knockouts persisted during exposure to submicromolar Ca^{2+}, even though this treatment destroyed the tip links. We conclude that the Tmc isoforms do not themselves constitute the MT channel but are essential for targeting and interaction with the tip link. Changes in the MT conductance and Ca^{2+} permeability observed in the absence of Tmc1 mutants may stem from loss of interaction with protein partners in the transduction complex.

The Journal of General Physiology

INTRODUCTION

Sensory receptors convert extrinsic stimuli into receptor potentials through direct or indirect activation of ion channels. Vertebrate mechanotransduction is the least understood of the sensory modalities, and the molecular composition of the underlying ion channel has yet to be definitively identified. Many of the properties of the mechanotransducer (MT) ion channels of inner ear hair cells have been characterized (Fettiplace, 2009; Peng et al., 2011), but the molecular identity of these channels remains controversial. Cochlear hair cells detect sound by vibrations of their stereociliary bundles, which apply force to the MT channels via tip links, extracellular filaments that connect the top of each stereocilium with the side wall of its taller neighbor (Pickles et al., 1984; Furness and Hackney, 1985). The tip links are composed of dimers of cadherin-23 at the upper end associated with dimers of protocadherin-15 at the lower end (Kazmierczak et al., 2007); the latter transmit force to MT channels localized at the tops of all but the tallest stereocilia (Beurg et al., 2009). A protein, TMHS (Lhfpl5), that may potentially couple the tip link to the MT channel has been identified (Xiong et al., 2012), and knocking out this protein reduces the MT channel conductance, suggesting that the channel's properties can be modified by other members of the transduction complex.

Mutations of Tmc1, a member of the transmembrane channel–like family, produce autosomal recessive profound deafness type DFNB7/11 and dominant progressive deafness type DFNA36 in humans. Equivalent mouse mutations include the "*dn*" and "*Beethoven*" mutations of the *Tmc1* gene, which cause profound or progressive hearing loss, respectively (Steel and Bock, 1980; Kurima et al., 2002; Vreugde et al., 2002; Marcotti et al., 2006). Recent work has shown that Tmc1 and Tmc2 are necessary for hair cell transduction: knocking out both isoforms abolishes MT currents in auditory and vestibular epithelia, a loss that can be rescued by exogenous expression of either Tmc1 or Tmc2 (Kawashima et al., 2011). Although these results argue for a fundamental role of Tmc's in hair cell mechanotransduction, they do not unequivocally establish them as ion channels. Heterologously expressed *Caenorhabditis elegans* Tmc1 has been reported to form a Na^+-sensitive ion channel (Chatzigeorgiou et al., 2013), but this has not been replicated for vertebrate isoforms. The Ca^{2+} permeability of the MT channel was altered in hair cells lacking Tmc1 or Tmc2 (Kim and

Correspondence to Robert Fettiplace: fettiplace@wisc.edu

Abbreviations used in this paper: MT, mechanotransducer; OHC, outer hair cell.

The Rockefeller University Press $30.00
J. Gen. Physiol. Vol. 142 No. 5 493–505
www.jgp.org/cgi/doi/10.1085/jgp.201311068

Fettiplace, 2013). Furthermore, here, we find that in Tmc1 knockouts, the unitary conductance of the MT channel is reduced. However, we still observed MT currents evoked by bundle displacements in mice with null mutations of both Tmc1 and Tmc2, although these currents had unusual properties. Our results argue that the Tmc's are likely to be accessory or trafficking proteins and not the pore-forming subunits of the MT channel.

MATERIALS AND METHODS

Preparation

MT currents were recorded in outer hair cells (OHCs) in isolated organs of Corti of mice between 0 and 10 d postnatal (P0 to P10, where P0 is the birth date) using methods described previously (Beurg et al., 2006; Kim and Fettiplace, 2013). Mutation in Tmc1 was achieved with *dn* mice (CBA.Cg-*Tmc1*^{dn}/AjgJ; The Jackson Laboratory), which contain a deletion of exon 14 and are on a CBA/J background. The Tmc2 mutant (B6;129S5-*Tmc2*^{tm1Lex}/Mmucd), in which exon 1 is deleted, was obtained from the Mutant Mouse Regional Resource Center (University of California, Davis). The Tmc2 mutant was back crossed over multiple generations with CBA/J mice to put it on the same background as the Tmc1 mutant. Control measurements were made on CD-1 outbred mice or on Tmc1 or Tmc2 heterozygotes. Mice were genotyped from tail clips using primer sets suggested by the suppliers.

Mice were killed by decapitation using methods approved by the Institutional Animal Care and Use Committee of the University of Wisconsin-Madison according to current National Institutes of Health guidelines. Excised cochlear turns, either apex or base (originating at ∼0.2 or 0.7 of the distance along the cochlea from the apex), were immobilized under strands of dental floss in a recording chamber mounted on a microscope (Axioskop FS; Carl Zeiss) and viewed through a 40× water-immersion objective. The chamber was perfused with artificial perilymph of the following composition (mM): 150 NaCl, 6 KCl, 1.5 $CaCl_2$, 2 Na-pyruvate, 8 D-glucose, and 10 Na-HEPES, pH 7.4 (osmolarity of ∼315 mOsm/l). The solution around the hair bundle was controlled using a local puffer pipette, and this was used to change the Ca^{2+} concentration to one containing different Ca^{2+} concentrations of (mM) 0.02 (buffered with 4 HEDTA), 0.07, 0.35, 6, 20, and 100. For the higher concentrations (6 and 20 mM), the NaCl concentration was reduced to keep the osmolarity constant at ∼315 mOsm/l. At the highest concentration, the solution contained (mM): 100 $CaCl_2$, 20 *N*-methylglucamine, 6 Tris, and 10 glucose, adjusted with HCl to pH 7.4 and supplemented with D-glucose to give an osmolarity of ∼315 mOsm/l. The local puffer pipette was also used to apply MT channel blockers (dihydrostreptomycin [Sigma-Aldrich] and FM1-43 [Life Technologies]).

Electrical recordings and stimulation

Recordings were made with borosilicate patch electrodes filled with a solution containing the following (mM): 135 CsCl, 3 MgATP, 10 Tris phosphocreatine, 1 EGTA, and 10 Cs-HEPES, pH 7.2 (∼298 mOsm/l), connected to an amplifier (Axopatch 200A; Molecular Devices) with an output filter at 10 kHz. Membrane potentials were corrected for liquid junction potentials and for voltage drop across the uncompensated series resistance. Most voltage-clamp protocols are referred to a holding potential of −84 mV. Hair bundles were mechanically stimulated with a fluid jet from a pipette (tip diameter of 10–15 µm) driven by a 25-mm-diameter piezoelectric disc (Johnson et al., 2011). The position of the stimulating pipette was adjusted to elicit a maximal MT current. The stimulus was usually a 35-Hz sinusoid, but sometimes the fluid jet was driven with voltage steps filtered at 1 kHz (Kros et al., 2002). In some experiments, the bundle motion produced by fluid stimulation was calibrated by projecting an image of the bundle onto a pair of photodiodes (LD 2–5; Centronics) at a total magnification of 340. Current–voltage relationships and MT current–displacement curves were determined from automated protocols generated by a Cambridge Electronic Design (CED) Power1401 interface driven by a PC. Data were digitized with the CED interface, and the results were analyzed with IGOR Pro v6 (WaveMetrics). Unless otherwise stated, values are given as mean ± 1 SEM, and $P < 0.02$ indicates statistical significance on a two-tailed Student's *t* test. All experiments were performed at room temperature of 21–25°C.

Reversal potentials (V_{REV}) and relative Ca^{2+} permeability (P_{Ca}/P_{Cs}) were determined (Kim and Fettiplace, 2013) by bathing cells in an extracellular solution containing the following (mM): 100 $CaCl_2$, 20 *N*-methylglucamine, 6 Tris, and 10 glucose, adjusted with HCl to pH 7.4, in both the fluid jet and the puffer pipette. Reversal potentials were corrected for a liquid junction potential of 9 mV. The relative Ca^{2+} permeability, P_{Ca}/P_{Cs}, was calculated from the Goldman–Hodgkin–Katz equation:

$$P_{Ca}/P_{Cs} = \left\{a_1\left[Cs^+\right]\right/4a_2\left[Ca^{2+}\right]\right\} \times \left\{\exp\left(V_{REV}\,F/RT\right)\right\} \times \left\{1+\exp\left(V_{REV}\,F/RT\right)\right\},$$

where RT/F has its usual meaning, with a value at room temperature of 25.7 mV; $[Cs^+]$ and $[Ca^{2+}]$ are the concentrations of Cs^+ intracellularly (142 mM) and Ca^{2+} extracellularly (100 mM), and a_1 and a_2 are activity coefficients for Cs^+ (Partanen, 2010) and Ca^{2+} (Rard and Clegg, 1997), respectively.

To isolate single MT channels in a whole-cell recording mode, saline with submicromolar free Ca^{2+} (composition [mM]: 140 NaCl, 6 KCl, 1 $CaCl_2$, 5 1,2-bis(o-aminophenoxy) ethane-*N*,*N*,*N*9,*N*9-tetraacetic acid [BAPTA], 8 glucose, and 10 Na-HEPES, pH 7.4; free Ca^{2+} of 0.05 µM) was pressure-ejected onto the hair bundles for 10–20 s to sever almost all of the tip links (Beurg et al., 2006). Single-channel responses were elicited by hair bundle deflections with a glass stylus, polished to ∼3-µm tip diameter, and driven by a piezoelectric stack actuator (PA8/12; piezosystems jena GmbH). The driving voltage to the actuator was filtered at 3 kHz, yielding a step displacement with a rise time of ∼100 µs. Single-channel currents were filtered at 5 kHz.

Scanning electron microscopy

Scanning electron micrographs of cochlear hair bundles from P5 and P6 Tmc1−/−Tmc2−/− or heterozygote mice were obtained after preparing samples using the repeated osmium–thiohydro–carbazide technique modified from Furness and Hackney (1986). Mice were killed by decapitation using methods approved by the Institutional Animal Care and Use Committee of the University of Wisconsin-Madison. Apical low frequency and basal high frequency cochlear turns were isolated after removal of the tectorial membrane, fixed in 2.5% glutaraldehyde in 0.1 M of sodium cacodylate buffer, pH 7.4, plus 2 mM $CaCl_2$ for 1 h, and then stored at 4°C in a 10% dilution of the original fixative. To examine the effects of exposure to the submicromolar Ca^{2+} solution thought to sever the tip links (Assad et al., 1991; Goodyear et al., 2005), P6 cochleas were treated for 5 min after excision in a solution composed of the following (mM): 140 NaCl, 6 KCl, 1.0 $CaCl_2$, 5 BAPTA (giving a free Ca^{2+} of 0.05 µM), 8 glucose, and 10 Na-HEPES, pH 7.4. Fixed cochlear turns were later postfixed for 1 h at room temperature in 1% osmium tetroxide (OsO_4) in sodium cacodylate buffer, washed in the buffer, and placed in a saturated filtered solution of thiocarbohydrazide for 20 min and washed in water. The tissue was then immersed in OsO_4 for 2 h, washed and placed in the thiocarbohydrazide for 20 min before washing and a third immersion in OsO_4 for another 2 h, followed by a final wash in water and transfer

to 70% ethanol. It was then dehydrated through an ethanolic series, critical point dried from liquid CO_2, mounted on SEM specimen stubs using carbon double-sided adhesive discs, and examined in a field emission scanning electron microscope (S-4500; Hitachi) operated at an accelerating voltage of 5 kV.

For quantitative analysis of tip-link survival, a region of hair bundles was selected randomly at low power from the apical turn, and then individual hair bundles of OHCs from each of the three rows were examined at high magnification (45,000). The number of stereocilia in all three ranks (N) was counted on screen, followed by the number of tip links visible (n_L). From these data, the proportion of tip links surviving was calculated ($n_L/N*0.67$, where 0.67 represents the expected proportion of tip-link sites per bundle assuming three serried rows of stereocilia). The three groups, or heterozygotes and Tmc1−/−Tmc2−/− with or without prior BAPTA treatment, were compared statistically using ANOVA, followed by pairwise comparison using the Wilcoxon sign-rank test.

RESULTS

MT currents in OHCs of double knockouts

MT currents in OHCs of neonatal Tmc1−/−Tmc2−/− mice could be routinely recorded in response to sinusoidal displacements of the hair bundle produced by a fluid jet (Fig. 1 A). The current amplitude assayed at a holding potential of −84 mV was variable and for P4–P6 mice ranged from ∼0.05 to 0.8 nA between preparations. However, the characteristics of the current were unusual in that it was activated by the opposite polarity of bundle motion compared with heterozygotes plus single knockouts (Fig. 1 A) or to wild type (Kim and Fettiplace, 2013). The current was evoked by displacements of the hair bundle away from the tallest edge rather than toward it as in wild-type hair cells. It will subsequently be referred to as a "reverse-polarity" current to denote its preference for a stimulus of reversed polarity. The polarity was normally established by stimulating with the fluid jet positioned adjacent to the shortest edge of the bundle, but if the fluid jet was placed on the opposite side of the bundle, the same polarity was observed and remained opposite to that seen in normal animals. Thus, it still displayed directional selectivity with respect to bundle motion. The reverse-polarity current was also less sensitive than normal and for large displacements had a "V"-shaped appearance in contrast to the square shape of the saturated currents in wild type (Fig. 1 A). The current–displacement relationships showed little evidence of saturation (Fig. 1 B). Although it was possible to image the hair bundle to infer the current–displacement relationship, the meaning of the bundle displacement in evoking the reverse-polarity current is unclear. In some cells, during repetitive stimulation the hair bundle became disorganized and sometimes almost completely destroyed, but this was not correlated with rundown of current, suggesting the reverse-polarity response does not require an intact bundle.

The current could also be elicited by step displacements of the hair bundle using the fluid jet (Fig. 2, A and B). Control currents responded to movements toward the tallest edge of the bundle and showed fast activation (Fig. 2 A) and adaptation, with the shapes of the currents being similar to those reported previously (Beurg et al., 2006). Depolarization to +76 mV, which minimizes Ca^{2+} influx, slowed the adaptation (but did not fully extinguish it), and there was an increase in the MT current activated at rest. Because of the low-pass filtering imposed by the fluid jet (Dinklo et al., 2007), the adaptation was slower than that using a glass stylus driven by a piezoactuator (Kennedy et al., 2003; Stauffer and Holt, 2007), and

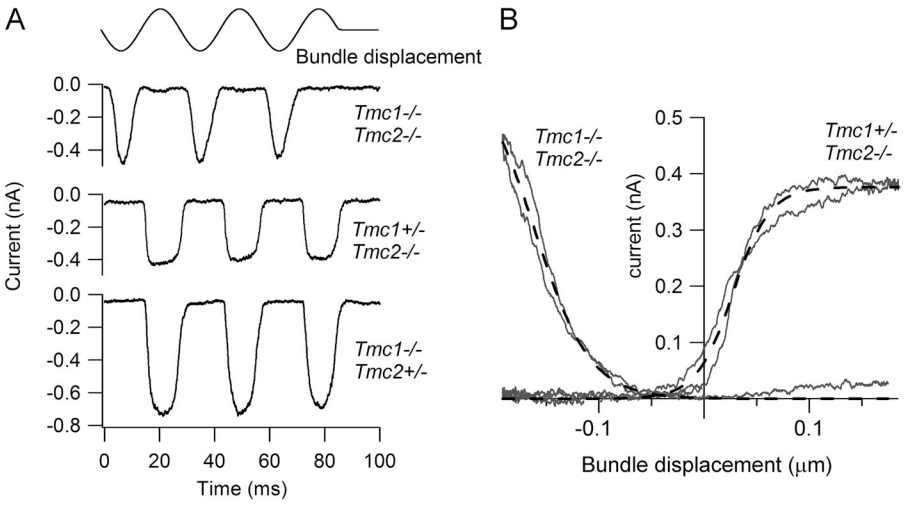

Figure 1. Reverse-polarity MT currents in OHCs of Tmc1−/−Tmc2−/− double knockouts. (A) Examples of MT currents in response to sinusoidal deflections of the hair bundle for a P2 Tmc1−/−Tmc2−/− double knockout and for P2 Tmc1−/−Tmc2+/− and P3 Tmc1+/−Tmc2−/− mice. All recordings from basal OHCs at a holding potential of −84 mV; stimulus monitor, the driving voltage to the fluid jet, is shown at the top. In this and subsequent figures, a positive driving voltage denotes displacement toward the tallest edge of the hair bundle. Note that the double knockout response occurs on the opposite phase of the stimulus to those in the heterozygote plus single knockouts. (B) Current–displacement (I-X) relationships for the Tmc1−/−Tmc2−/− and for the Tmc1+/−Tmc2−/− recordings. MT current over the first cycle of the response was plotted against bundle displacement, inferred by calibrating hair bundle motion (see Materials and methods). Dashed lines are fits with single-state Boltzmann: $I = I_{max}/(1 + \exp(-((X-X_1)/X_2)))$, where X_1 is the half-activation displacement, X_2 is rate, and I_{max} is maximum current. Parameter values for Tmc1+/−Tmc2−/−: I_{max}, 0.38 nA; X_1, 27 nm; X_2, 18 nm. Parameter values for Tmc1−/−Tmc2−/−: I_{max}, 0.66 nA; X_1, −165 nm; X_2, −33 nm.

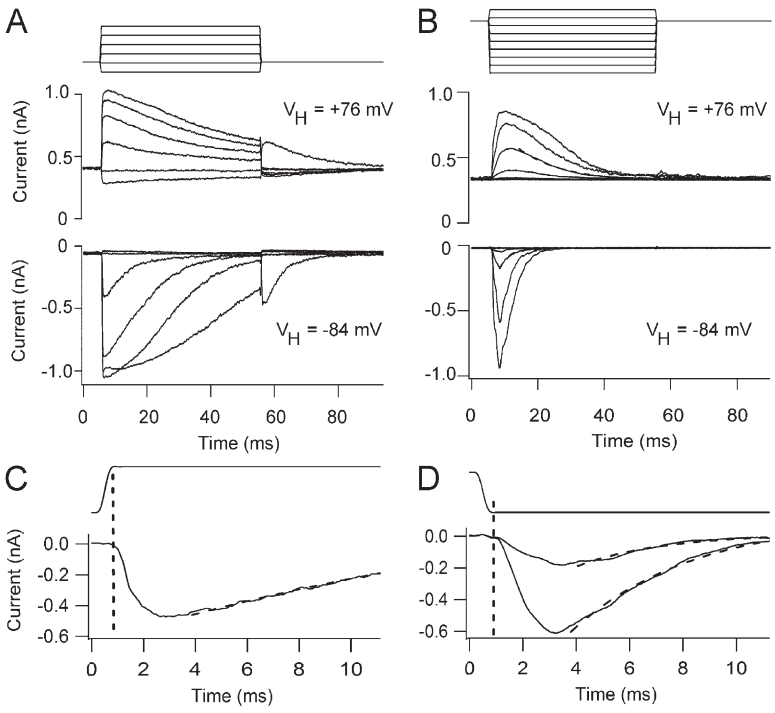

Figure 2. MT currents in response to fluid jet step stimuli. (A) Family of MT currents evoked by step deflections of the hair bundle in an apical OHC from a P5 Tmc1+/−Tmc2+/− heterozygote at +76 mV (top) and −84 mV (bottom). (B) Family of MT currents evoked by hair bundle steps in a P4 apical OHC from a Tmc1−/−Tmc2−/− double knockout at +76 mV (top) and −84 mV (bottom). The driving voltage to the fluid jet, low-pass filtered at 1 kHz, is shown above the currents. (C) Onset of one of the currents in a P5 heterozygote apical OHC shown on a faster time base; dashed line, fit with a decay time constant of 16 ms. (D) Onset of two currents of a P4 apical OHC from a Tmc1−/−Tmc2−/− double knockout on a faster time base; dashed lines, fits with time constants of 3.3 and 6.3 ms. Note the response delay is similar in the heterozygote and double knockout.

at −84 mV had a time constant of several milliseconds. Similar MT currents could also be evoked in the double knockouts, but responses were obtained solely for larger bundle movements of the opposite polarity, away from the tallest edge of the bundle (Fig. 2 B). This might explain why they were not seen in the previous work (Kawashima et al., 2011), because, with the piezoactuator-driven glass stylus used in those experiments, it may have been difficult to pull the bundle back toward its shortest edge without the probe detaching. The currents also showed relatively fast activation followed by a decline in the current back to the baseline (Fig. 2 B), with a mean time constant of 2.9 ± 0.3 ms (n = 5 OHCs), but in contrast to the controls never showed a sustained response. The decline in the current during the step, although slowed, was still pronounced at +76 mV, implying that it is not regulated primarily by Ca^{2+} influx. In support of that notion, exposure to the submicromolar Ca^{2+} buffered with BAPTA (later be shown not to abolish the MT currents in the double knockouts) had no effect on the decline in the current during the maintained stimulus. The decay time constant was 3.2 ± 0.1 ms (n = 4 OHCs), which was not significantly different from the value in normal saline (P = 0.40).

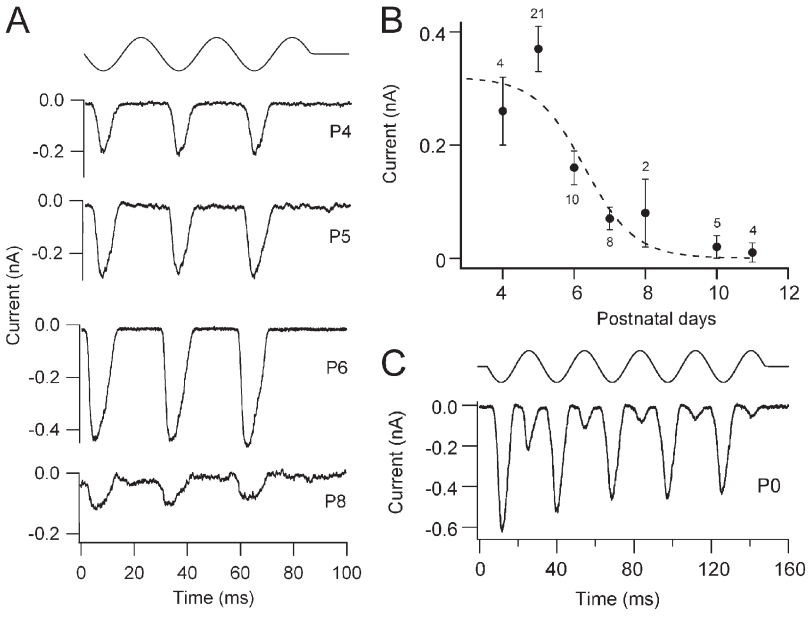

Figure 3. Development of reverse-polarity MT currents in Tmc1−/−Tmc2−/− double knockouts. (A) Examples of reverse-polarity MT currents in apical OHCs of Tmc1−/−Tmc2−/− double knockout mice at four postnatal ages, given beside each trace. (B) Plot of the mean reverse-polarity MT current (±SEM) against postnatal age; numbers of cells are given above points. Time course of current, I, fitted with a sigmoidal decay: $I = I_{max}/(1 + \exp(-(T-T_{0.5})/T_R))$, with I_{max} = 0.32 nA, decay half-time $T_{0.5}$ = 6.3 ± 0.6 d, and rate T_R = 0.7 d. (C) Example of MT current in Tmc1−/−Tmc2−/− in a P0 OHC; the reverse-polarity component of the two-harmonic response is larger.

In wild-type mice, the OHC MT current develops over the first few days after birth (Lelli et al., 2009; Kim and Fettiplace, 2013) and at the apex peaks at about P4–P5 as the hair bundle achieves its mature V-shaped appearance. The reverse-polarity currents in the double knockouts were initially cataloged from P4 onward and found to decline in amplitude after P6 (Fig. 2 B), and few cells showed signs of such current at P10 or later. The time course in the decline of the current with age closely mirrors that seen in the Tmc1−/− (Fig. 3 of Kim and Fettiplace, 2013). Fits to the time course gave a half-amplitude at 6.3 ± 0.6 d (±1 SD; Fig. 2 B) compared with 6.7 ± 0.2 d seen in the Tmc1−/− apical OHCs. In view of the scatter in the points, largely attributable to variation in current amplitude from one preparation to another, there is little difference between these two values. Large currents evoked by bundle displacement could be recorded in OHCs of double knockouts at even earlier ages from P0 onwards, but in most cells studied, these currents exhibited two-harmonic responses in that they occurred on both phases of a sinusoidal stimulus (Fig. 3 C). At this age up to 2 d postnatal, the mean amplitude of the reverse-polarity component was 0.23 ± 0.08 nA (n = 8 OHCs; P0–P2). Because of the more complex pattern of response, the reverse-polarity current amplitudes were not included in the developmental plot in Fig. 3 B. It is worth noting that a lack of directional selectivity is also seen in the wild-type OHCs during the first few postnatal days (Waguespack et al., 2007). In our recordings, two-harmonic currents were seen in four out of five OHCs at P0 and four out of nine OHCs at P1. The meaning of such responses is unclear but may be related to refinement of the inter-stereociliary links (Goodyear et al., 2005), which initially run in multiple directions, or to the presence of mechanically sensitive microvilli on the apical membrane of the hair cell. At the ages where most of the measurements were made (P4–P6), the microvilli had been reabsorbed (Fig. 6 A). These results indicate that OHCs in double Tmc1−/−Tmc2−/− knockout mice possess substantial MT currents of similar amplitude to those in wild type at the same age.

Block and permeability of reverse-polarity MT currents

To address whether the MT channels occurring in the double knockouts had the same ionic properties as those normally present in wild-type OHCs, we next examined the ionic permeability and block of the reverse-polarity currents. The currents were reversibly blocked by FM1-43 (Fig. 4 A), which is known to block the OHC MT currents (Gale et al., 2001). With 5 µM, the reverse-polarity current was reduced to 0.37 ± 0.09 (n = 4) of that in the control and wash, a value virtually identical to that reported by Gale et al. (2001) at a holding potential of −104 mV, at which the K_I was 2.4 µM. The reverse-polarity current

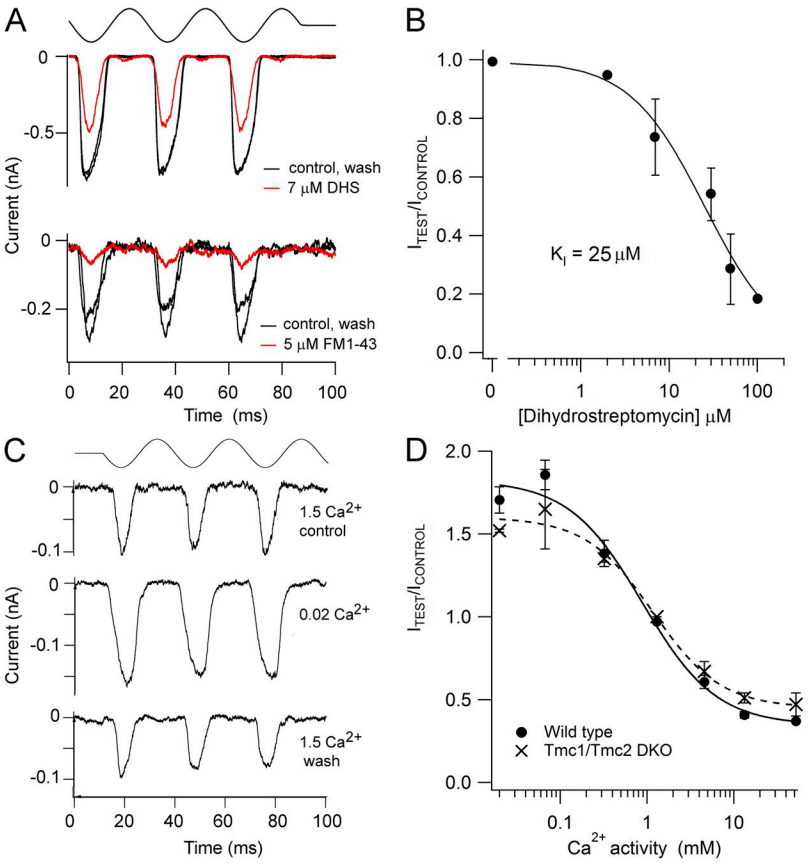

Figure 4. Permeability and block of the reverse-polarity MT current in Tmc1−/−Tmc2−/−. (A) Current is reversibly reduced by 5 µM FM1-43 and by 7 µM dihydrosteptomycin in P5 apical OHCs. (B) Dose–response relationship for block of the reverse-polarity current by dihydrosteptomycin, with two to three OHCs assayed at each concentration. Results fit with a Hill equation with a half-blocking concentration, K_I, of 25 ± 6 µM and a Hill coefficient of 1.02 ± 0.2. Note the break in the abscissa at 0.2 µM. (C) Reducing extracellular Ca^{2+} bathing the hair bundle from 1.5 mM (perilymph) to 0.02 mM (endolymph) augments the reverse-polarity MT current in a P6 apical OHC. Top traces in A and C are the driving voltage to the fluid jet stimulator. (D) Plot of mean MT current against the Ca^{2+} activity in the saline bathing the hair bundle in wild-type (closed circles) and Tmc1−/−Tmc2−/− (crosses) apical OHCs. The measurements were performed by changing the bundle perfusate from saline with 1.5 mM Ca^{2+} to one containing the test Ca^{2+} concentration, and then washing in 1.5 mM Ca^{2+}. All MT currents are normalized to that in 1.5 mM Ca^{2+} control and wash. 4–10 cells were averaged for the wild type, and 2–5 cells were averaged for the Tmc1−/−Tmc2−/−. Points were fitted with Hill plots with half-blocking concentration: K_I = 0.9 ± 0.3 mM and Hill coefficient of 1.0 ± 0.3 for wild type, and K_I = 1.2 ± 0.3 mM and Hill coefficient of 1.1 ± 0.3 for Tmc1−/−Tmc2−/−.

was also blocked by dihydrostreptomycin, with the dose–response relationship (Fig. 4 B) having a half-blocking concentration of 25 ± 6 µM, which is comparable to the value reported for wild-type OHCs (~10 µM; Marcotti et al., 2005). In addition, the reverse-polarity currents were blocked by extracellular Ca^{2+} (Fig. 4 C), as has been found for MT channels in wild-type mice and in auditory hair cells of (nonmutant) turtles and rats (Ricci and Fettiplace, 1998; Beurg et al., 2006). Reducing extracellular Ca^{2+} from 1.5 to 0.02 mM, its concentration in endolymph, eliminated the block and increased the current amplitude 1.5-fold (mean increase of 1.52 ± 0.01; $n = 3$). The change in current amplitude with respect to that in 1.5 mM Ca^{2+} was titrated against the extracellular Ca^{2+} concentration to generate a blocking relationship (Fig. 4 D, crosses). The Ca^{2+} concentration for half-block, K_I, was 1.2 ± 0.3 mM (±SD), and the Hill coefficient was 1.1 ± 0.3. For comparison, the equivalent values in apical OHCs of wild-type mice of the same age (Fig. 4 D, closed symbols) were 0.9 ± 0.3 mM for K_I and 1.0 ± 0.3 for the Hill coefficient. These experiments suggest that the normal and reverse-polarity MT currents respond similarly to the blocking agents used.

We next examined the ionic permeability of the channels. The current–voltage relationship in extracellular saline containing 1.5 mM Ca^{2+} was approximately linear (not depicted) and reversed at +6.1 ± 0.5 mV ($n = 4$). This value is not significantly different ($P = 0.33$) from the reversal potential measured under the same conditions in wild type (mean = 4.7 ± 1.1 mV; $n = 5$). The reversal potential is consistent with the underlying ion channel being a nonselective cation channel, as is the case for the normal MT channel (Ohmori, 1985; Kros et al., 1992). A reversal potential of +6 mV with the solution compositions used here corresponds to a P_{Na}/P_{Cs} of ~1.1. The permeability characteristics were investigated further by determining the relative Ca^{2+} selectivity, as was done with the single Tmc knockouts (Kim and Fettiplace, 2013). Reversal potentials measurements were made with 100 mM Ca^{2+} in the external solution and 142 mM of total Cs^+ in the intracellular solution as the principal conducting ions, neglecting the contributions from the small amounts of Tris and *N*-methylglucamine. OHC bundles were vibrated sinusoidally with a fluid jet, and the membrane potential was ramped from −150 to +100 mV (Fig. 5 A). The reversal potential at both the apex and base were >10 mV more negative relative to the heterozygote littermates (Fig. 5, B and C). The mean Ca^{2+} reversal potentials for the reverse-polarity MT channels in the double knockouts were 10.9 ± 0.6 mV ($n = 6$; P5 apical OHCs) and 9.9 ± 0.5 mV ($n = 3$; P2 basal OHCs). The respective P_{Ca}/P_{Cs} permeability ratios were calculated as 1.9 ± 0.07 at the apex and 1.8 ± 0.04 at the base. These values are significantly smaller ($P < 0.001$) than those in wild-type or single knockouts, all of which lie between 3.7 and 6.3. The equivalent reversal potentials in the OHCs of wild-type or single knockouts were between 22 and 28 mV depending on the condition (Kim and Fettiplace, 2013). Collectively, the results indicate that although some aspects of the underlying reverse-polarity current resemble those of the wild type, there are differences in the Ca^{2+} permeability.

The effects of tip-link destruction

The hair bundles of apical OHCs in the double knockouts were relatively intact at the age (P4–P6) at which most of the recordings were made (Fig. 6 A). The most significant abnormality was that the bundles had more rounded sides compared with the straight wings of the wild type or heterozygotes. Nevertheless, they possessed tip links and also still retained side-to-side links between adjacent stereocilia (Fig. 6 B); the latter are sometimes

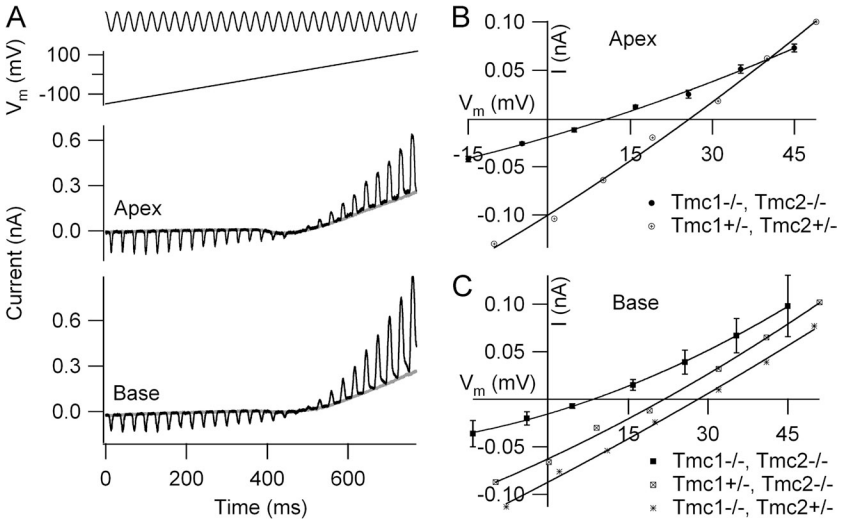

Figure 5. Ca^{2+} permeability of OHC MT currents. (A) Examples of reverse-polarity currents in a P5 apical OHC and a P2 basal OHC of Tmc1−/−Tmc2−/− mice. Hair bundle stimulated continuously with a sinusoidal fluid jet (top trace) during a voltage ramp from −150 to +100 mV (second trace), apical and basal currents (third and fourth traces). Extracellular solution contains 100 mM $CaCl_2$ (see Materials and methods for full composition). (B) Current–voltage plots around reversal for apical OHCs of Tmc1−/−Tmc2−/− (mean ± SEM; $n = 6$, P5) and Tmc1+/−Tmc2+/− heterozygous P5 littermates. (C) Current–voltage plots around reversal for basal OHCs of Tmc1−/−Tmc2−/− (mean ± SEM; $n = 3$, P2), Tmc1+/−Tmc2−/−, and Tmc1−/−Tmc2+/− P3 mice. Note that the double knockout MT currents at both apex and base reverse >10 mV more negative than the heterozygotes or single knockouts, implying a smaller Ca^{2+} permeability.

referred to as "transient lateral links" and are thought to disappear in mice by P9 (Goodyear et al., 2005). As in the wild type (Assad et al., 1991; Goodyear et al., 2005; Furness et al., 2008; Indzhykulian et al., 2013), the majority of the tip links could be destroyed by exposure to submicromolar Ca^{2+} buffered with BAPTA (Fig. 6 D). Tip-link survival in OHCs was quantified (see Materials and methods) by counting in scanning electron microscope images the visible tip links and the number of stereocilia per bundle, and then assuming that the maximum number of tip links is two thirds the number of stereocilia. The fraction of tip links visible compared with the expected maximum in each cell (±SD) was: 0.37 ± 0.11 (n = 20 cells from Tmc1+/−Tmc2+/− heterozygotes; range = 0.20–0.67); 0.39 ± 0.13 (n = 20 cells from Tmc1−/−Tmc2−/− double knockouts; range = 0.15–0.65); and 0.10 ± 0.06 (n = 16 cells from double knockouts after 5 min of BAPTA exposure; range = 0.04–0.2). The heterozygotes and double knockouts were not significantly different (Wilcoxon test; P = 0.2), but the double knockouts with or without prior BAPTA treatment were significantly different ($P = 5 \times 10^{-9}$). The less than full complement of tip links in the absence of BAPTA may be an artifact of the specimen preparation, but why some tip links seem to remain after BAPTA is unclear. Given the large number of lateral links in the neonatal mice, it is possible that some lateral links near the tops of the stereocilia were misidentified as tip links. Nevertheless the results argue for a substantial loss of tip links after BAPTA treatment.

In contrast to the susceptibility of the tip links, the reverse-polarity MT currents in the Tmc1−/−Tmc2−/− were completely resistant to the BAPTA treatment, and indeed the amplitude of the MT current approximately doubled during BAPTA perfusion (Fig. 6 C); the increase in amplitude can be explained by complete removal of Ca^{2+} block of the channels as documented above. The effect was reversible, and the size of the current decreased again on washing with normal 1.5 mM Ca^{2+} saline. The ratio of current amplitudes in BAPTA compared with those in control saline was 2.2 ± 0.2 (n = 4). The simplest conclusion from these observations is that the reverse-polarity currents, compared with wild types, are not coupled to bundle motion by force delivered through the tip links.

The use of BAPTA treatment to distinguish the normal and mutant MT currents was also effective in the early neonatal wild type or heterozygotes. Fig. 7 shows a recording from an early postnatal OHC, which initially gave a normal polarity response to bundle deflection. The MT current disappeared immediately after starting BAPTA perfusion, but as the BAPTA perfusion was continued, a reverse-polarity current appeared and then grew over 5–8 min. The existence of the reverse-polarity current here indicates that it is not an artifact of the double knockout. This type of behavior was seen in five OHCs tested during the early postnatal stage (P0–P4). In one recording, both the in-phase and reverse-phase currents were >80% blocked by 100 µM dihydrostreptomycin, indicating a similar sensitivity to this agent. It should be noted that Indzhykulian et al. (2013) have shown recovery of

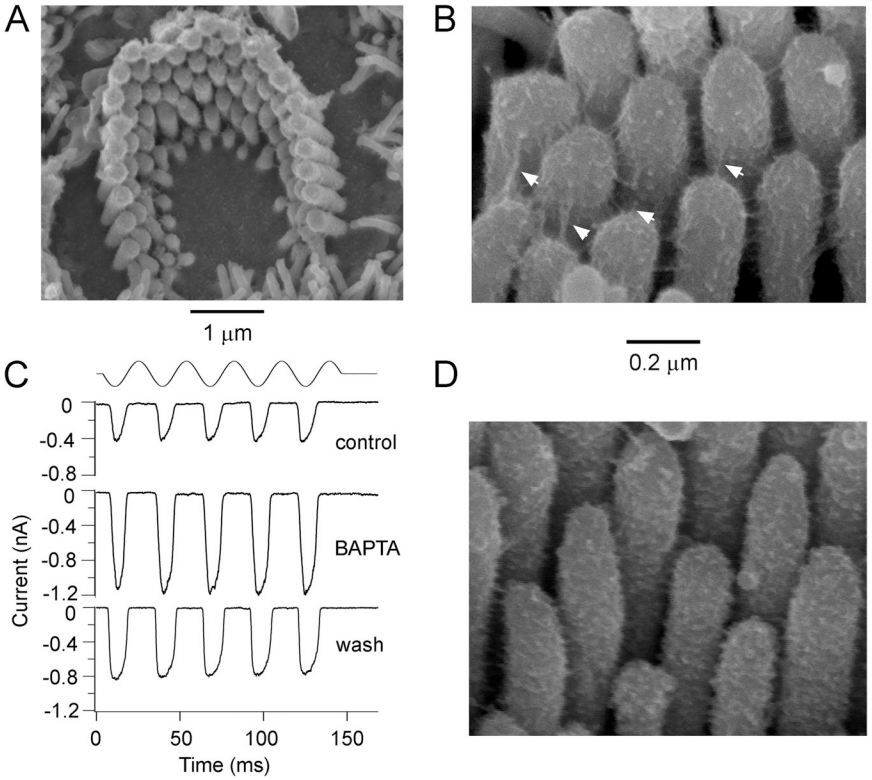

Figure 6. Apical OHC hair bundles and tip links in Tmc1−/−Tmc2−/−. (A) Scanning electron micrograph of an apical OHC bundle from a P6 double knockout showing an intact but rounded bundle. (B) High power scanning electron micrograph of the stereocilia of a P6 OHC bundle showing the tip links (arrowed) and interstereociliary side-to side links. (C) Reverse-polarity MT currents in a P5 apical OHC in a control 1.5 mM Ca^{2+} saline, during exposure to submicromolar Ca^{2+} solution buffered with 5 mM BAPTA, and after washing with the control saline. (D) High power scanning electron micrograph of the stereocilia of a P5 OHC bundle after the preparation was treated with 5 mM BAPTA for 5 min before fixation. Note the substantial loss of tip links, although some side-to-side links remain.

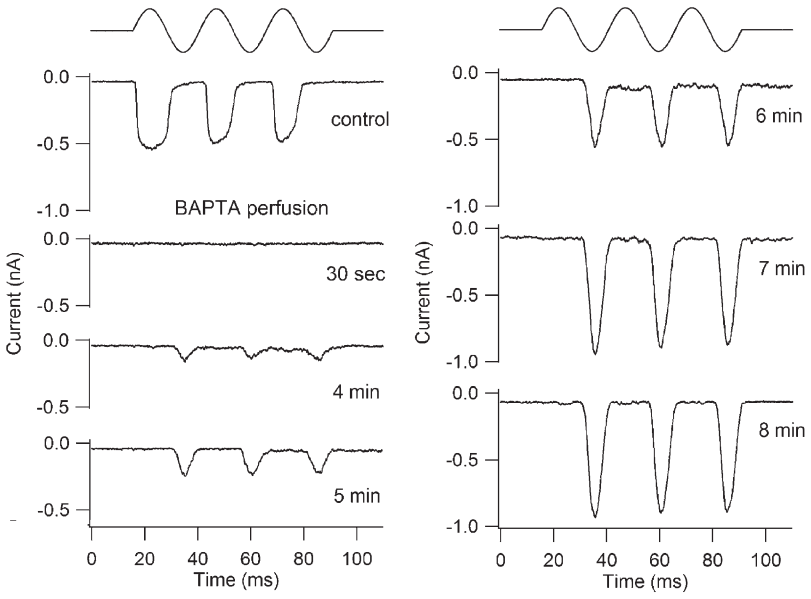

Figure 7. Effects of sustained perfusion of BAPTA on OHC MT currents. Examples of responses to sinusoidal fluid jet stimulation before and during perfusion with BAPTA in a P1 Tmc1+/−Tmc2+/+ OHC; numbers beside traces give the time after the start of BAPTA perfusion. Initially (control), an MT current of conventional polarity was recorded. After the onset of BAPTA perfusion at 0 s, the normal MT current disappeared, and thereafter, the reverse-polarity current appeared and grew to attain a maximal amplitude after 8 min.

MT currents after BAPTA treatment, but these were recorded >1 h after tip-link destruction by brief BAPTA exposure and were of normal polarity. Those currents were attributed to transient formation of anomalous links composed only of protocadherin-15.

Single-channel conductances in Tmc knockouts

Measurements of single-channel currents in wild type and Tmc nulls were performed to investigate the ion conduction pathway as a gauge of the pore structure. Single channels could be characterized in the whole-cell recording mode after destruction of the majority of the tip links by brief perfusion with submicromolar Ca^{2+} buffered with BAPTA (Assad et al., 1991; Crawford et al., 1991; Indzhykulian et al., 2013). Examples of such channels and their mechanosensitivity in OHCs from apical and basal turns of wild-type mice are shown in Fig. 8. Hair bundles were stimulated with a glass probe driven by a

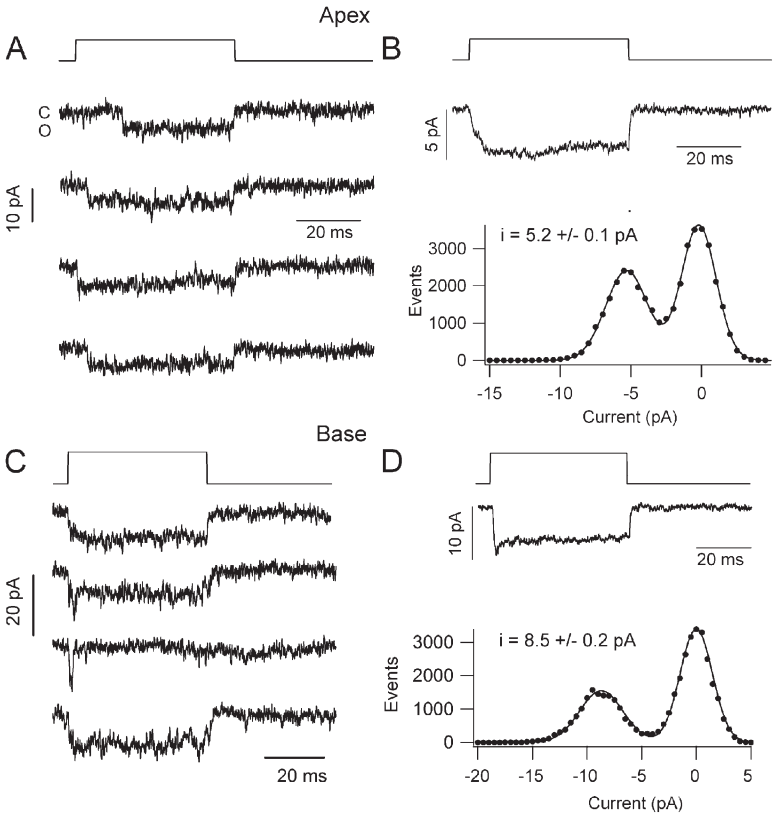

Figure 8. Single MT channel currents in wild-type OHCs. (A) Examples of single-channel currents in a P4 apical OHC recorded in whole-cell mode with a holding potential of −84 mV; hair bundle deflected by a glass probe driven by a piezoactuator, time course shown above, displacement of ∼0.2 µm. (B; Top) Ensemble average currents of 30 responses for apical OHC channels in A. (Bottom) Amplitude histogram of channel event for the cell in A. Points fitted with two Gaussians with peak at 0 and −5.2 pA. (C) Examples of single-channel currents in a P3 basal OHC with recording and hair bundle stimulation as in A. (D; Top) Ensemble average currents of 23 responses for channels from OHC in C. (Bottom) Amplitude histogram of the OHC events in C, fitted with two Gaussians with peaks at 0 and −8.6 pA. The leak current, usually <0.1 nA, was subtracted from the records before constructing single-channel histograms.

piezoactuator, and relatively large deflections of ~0.2 µm were generally used to produce maximal opening. In some cells, two or three open levels were detectable, but only those cells with a dominant single level were analyzed (Fig. 8, A and C). These generated ensemble averages synchronized to the displacement step and single peaks in the amplitude histogram (Fig. 8, B and D). The mean single-channel conductances were significantly different between apex and base (62 and 101 pS, respectively; $P < 0.02$; Table 1), consistent with a tonotopic gradient in conductance as seen in the turtle (Ricci et al., 2003) and rat (Beurg et al., 2006). No significant difference was seen between wild type and heterozygotes, or between wild type and Tmc2−/− (Table 1).

Single-channel currents in Tmc1−/− showed a smaller amplitude than either wild type or heterozygotes, although the basal current was slightly larger than the apical one. Nevertheless, the tonotopic gradient in the Tmc1 null was much diminished compared with the wild type (Fig. 9 and Table 1). The larger effect at the base is reminiscent of the consequences of Tmc1 knockout on the MT channel Ca^{2+} permeability, where the predominant effect was at the base (Kim and Fettiplace, 2013). Attempts were also made to isolate single-channel currents in the Tmc1−/−Tmc2−/− double knockout, but these were hampered by the failure of BAPTA to reduce the current size and hence the number of channels. On several occasions, channels were recorded under circumstances in which there was no obvious macroscopic current (Fig. 9, C and D). These channels responded to negative deflections of the hair bundle and, in contrast to the other channel recordings, displayed fast flickering with no maintained opening. Ensemble averages yielded a transient current resembling the macroscopic current in the double knockout (Fig. 2 B), with a decay time constant of ~3 ms and a unitary current of 5.5 ± 0.2 pA (Fig. 9 D). The properties of these channels are consistent with their underlying reverse-polarity response. In both wild type and double knockouts, a smaller 25-pS channel was also sometimes seen and was distinguished by its slow activation with onset and decay time constant of ~30 ms. Such a small, slow channel was previously reported in turtle hair cells (Crawford et al., 1991; Ricci et al., 2003), where it was referred to as a "subconductance state." It differs from the macroscopic MT current in the double knockout (Fig. 2 D) because it responds to the opposite stimulus polarity, it has a slow activation time course, and it is sustained for a step displacement. Based on this evidence, it is unlikely to make a contribution to the reverse-polarity current. Nevertheless, the characteristics of the small channel are included in Table 1.

DISCUSSION

Reverse-polarity MT currents

We have found that large, several hundred–picoampere receptor currents evoked by hair bundle displacements are still present during the first postnatal week in mice lacking both Tmc isoforms 1 and 2. This result differs from the findings of Kawashima et al. (2011), who saw no currents in double Tmc1/Tmc2 knockouts. The currents in our experiments were activated by negative deflections of the bundle and required a threshold displacement to appear (Fig. 1 B). They might therefore have been missed by stimulation with a glass probe placed against the shorter edge of the bundle, as was used by Kawashima et al. (2011), because, in our experience, such probes do not pull the bundle back well and tend to

TABLE 1

Single MT channel currents in mouse OHCs

Mice	Location	*I* channel	*G* channel	*n* traces	*n* cells, age
		pA	*pS*		
Wild type	Apex	5.2 ± 0.1[a,b]	62	50	5, P4–P5
Tmc1+/−	Apex	5.3 ± 0.1	63	41	4, P4
Tmc1−/−	Apex	4.1 ± 0.1[a]	49	93	6, P4–P5
Tmc2+/−	Apex	5.5 ± 0.3	65	13	4, P4
Tmc2−/−	Apex	5.2 ± 0.2	62	14	4, P4
Tmc1−/−Tmc2−/−	Apex	5.5 ± 0.1	65	56	4, P5–P6
Tmc1−/−Tmc2−/−	Apex	2.1 ± 0.03[c]	25	8	3, P6
Wild type	Base	8.5 ± 0.2[b,d]	101	80	14, P3
Tmc2−/−	Base	8.6 ± 0.2	102	37	5, P2–P3
Tmc2+/−	Base	8.1 ± 0.2	96	14	4, P2–P3
Tmc1−/−	Base	5.0 ± 0.1[d]	60	26	5, P2–P3

Location in cochlea at low frequency apex or high frequency base. *I* channel, single-channel currents measured at a holding potential of −84 mV from amplitude histograms, mean ± SEM; *G* channel, single-channel conductance; *n*, number of traces analyzed and cells characterized; P, postnatal age.

[a]Pairs of values were significantly different, $P < 0.02$.

[b]Pairs of values were significantly different, $P < 0.02$.

[c]MT channels of similar size were also occasionally seen in wild type and heterozygotes.

[d]Pairs of values were significantly different, $P < 0.02$.

become detached with negative stimuli. For this reason, we used a fluid jet stimulator (Kros et al., 1992) that, although having a slower onset, is able to push and pull the bundle equally well. The reverse-polarity current had some properties akin to the normal MT current in wild-type hair cells. It had a reversal potential close to 0 mV, as expected for a nonselective cation channel, and was susceptible to similar doses of blocking agents—FM1-43, dihydrostreptomycin, and extracellular Ca^{2+}—as the wild-type channel. It differed in requiring negative bundle displacements and strikingly persisted after exposure to BAPTA, which abolished many of the tip links. These two anomalous features are the same as those seen in certain protocadherin-15 mutations, which result in loss of tip links (Alagramam et al., 2011). In protocadherin-15 mutations causing tip-link loss, an MT current was recorded in response to negative bundle deflections. The simplest conclusion is that in the absence of Tmc1 and Tmc2, the MT channels are unable to connect with the tip link or be activated by its tensioning. However, this conclusion carries the implication that the Tmc proteins are not pore-forming subunits of the channel. The observation that reverse-polarity currents develop even in wild-type mice during continued exposure to BAPTA (Fig. 7) would be consistent with the incorporation of new MT channels in the membrane awaiting targeting to the tip-link region.

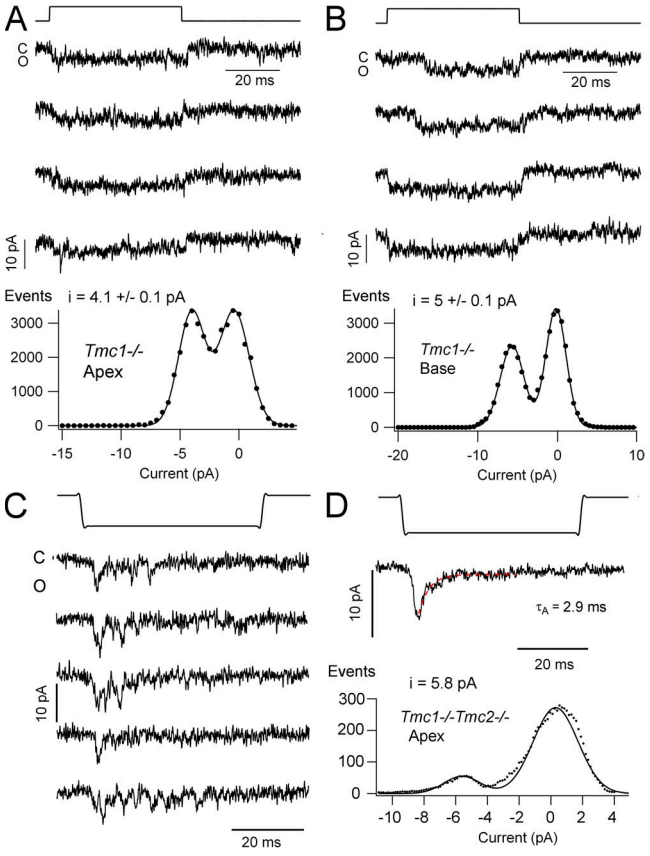

Figure 9. Single MT channel currents in Tmc mutants. (A) Examples of single-channel currents in a P5 apical OHC holding potential of −84 mV. Hair bundle deflection is shown above, and amplitude histogram of the OHC channel currents is shown below, fitted with two Gaussians with peaks at 0 and −4.1 pA. (B; Top) Single-channel currents in a P3 basal OHC with recording and stimulation conditions as in A. (Bottom) Amplitude histogram of the OHC channel currents fitted with two Gaussians with peaks at 0 and −5.0 pA. The tonotopic gradient in the wild type is much diminished in Tmc1−/−. (C) Single-channel currents in a P6 apical OHC of Tmc1−/−Tmc2−/− at −84 mV. (D; Top) Ensemble average current of 14 responses; decay fitted with an exponential time constant of 2.9 ms. (Bottom) Amplitude histogram of events in C, fitted with two Gaussians; channel amplitude of −5.8 pA.

Unanswered questions are how do the channels in the double mutants retain their sensitivity to bundle motion, and moreover, why do they become responsive to bundle displacements of the opposite polarity. There are two general possibilities: they could still be present in the stereocilia but floating free in the plasma membrane and not anchored to the cytoskeleton or the tip links, or they could be elsewhere in the bundle attached to inter-ciliary links that survive the BAPTA treatment. Reverse-polarity MT responses have been measured in developing zebrafish hair cells where they were attributed to the mechanosensitivity of the kinocilium before development of the tip links (Kindt et al., 2012). We were unable to demonstrate the persistence of kinociliary links, but some of the side-to-side links may have survived the BAPTA treatment (Fig. 6 D), and we cannot exclude their contribution to the reverse-polarity current. However, this conclusion seems inconsistent with our observation that the reverse-polarity current did not run down after repeated strong stimulation that disorganized and sometimes effectively destroyed the bundle. An alternative possibility is that in the double knockouts, MT channels are present on the apical membrane of the hair cell and at the base of the stereocilia. There has been a previous report of ion channels with large-conductance similar to MT channels on the apical surface of OHCs (Frolenkov, G.I., J. Gorelik, G.P. Richardson, C.J. Kros, A.J. Griffith, and Y.E. Korchev. 2004. 27th Association for Research in Otolaryngology MidWinter Meeting. Abstr. 1207). It is not obvious how such channels would be preferentially selective for negative hair bundle displacements, although one hypothesis is that they diffuse from the abneural margin of the hair cell apical membrane and accumulate at the base of each stereocilium on its abneural side awaiting transport up the stereociliary membrane. A similar directional transport from the hair cell apical membrane into the stereocilia has been observed for the CaATPase (Grati et al., 2006). They might therefore be activated by stretching of the membrane at the stereociliary base as the bundle rotates back toward the neural limb.

The role of Tmc proteins in hair cell transduction

There is no disputing that Tmc proteins are important for proper MT channel function and the adult mice are

deaf (Kawashima et al., 2011), but what then is their role if they are not pore-forming subunits of the MT channel? Even their presence in the stereocilia is uncertain. For example, antibody labeling indicated that in avian hair cells, Tmc2 was principally associated with the lateral membranes (Mutai et al., 2005). In contrast, hair cell transfection with Tmc2-GFP showed localization to the tops of the stereocilia (Kawashima et al., 2011). With neither labeling technique is there evidence of the subcellular localization of Tmc1. Two other Tmc isoforms, Tmc6 and Tmc8 (EVER1 and EVER2), may be involved in the regulation of cellular zinc homeostasis and have been suggested to complex with and activate the zinc transporter ZnT-1 in lymphocytes (Lazarczyk et al., 2008). They might therefore be auxiliary protein subunits of an ion transport mechanism and may also be responsible for targeting the transporter to the appropriate subcellular site. These attributes are similar to those of auxiliary proteins for other ion channels, a prime example being the TARP and cornichon (CNIH) proteins that influence both expression and channel properties of the AMPA receptors in the postsynaptic region of glutamate synapses on dendritic spines. For example, CNIH association modifies both the Ca^{2+} permeability and single-channel conductance of AMPA receptors (Coombs et al., 2012; Bats et al., 2013).

Based on our results, we hypothesize that the Tmc1 and Tmc2 isoforms are at the very least required for targeting the MT channel to the tops of the stereocilia where they can interact with other constituents of the transduction complex, including the tip link. Importantly, we suggest that such localization can modify the ion conduction properties of the channel. Our results demonstrate that in the absence of Tmc1, both the channel's Ca^{2+} permeability and its unitary conductance are changed, with these effects being most pronounced at the basal high frequency end of the cochlea. Modifications in Ca^{2+} permeability and unitary conductance have recently been reported for MT channels of inner hair cells in Tmc1 or Tmc2 single knockouts (Pan et al., 2013), and these results were used as evidence for the Tmc's being pore-forming subunits of the MT channel. However, such changes could also be accomplished by interactions with other members of the transduction complex, such as TMHS (Xiong et al., 2012). In the absence of interactions with protein partners in the transduction complex, the attributes of the reverse-polarity MT current documented here may represent the root properties of the ion channel. This channel has a P_{Na}/P_{Cs} of ~1.1 and a P_{Ca}/P_{Cs} of 1.9, and a few measurements indicate a unitary conductance of ~60 pS in 1.5 mM of extracellular Ca^{2+}, and in zero Ca^{2+} that conductance is doubled. These properties are comparable to those of a known vertebrate mechanosensitive cation channel, Piezo1 (Coste et al., 2010, 2012). Piezo1 has a P_{Na}/P_{Cs} of 1.1, a P_{Ca}/P_{Cs} of 1.9, and a unitary conductance of 30 pS in normal extracellular Ca^{2+} and 59 pS without Ca^{2+}, and it displays rapid and complete inactivation similar to that for the reverse-polarity current (Fig. 2 B). The similarities to Piezo1 provide only circumstantial evidence and other as yet unidentified channels may share such properties. Firm identification of the MT channel molecule will be needed to understand the mechanisms that regulate its properties along the cochlea's tonotopic axis.

We thank Walter Marcotti and Corné Kros for helpful discussions.

This work was funded by a grant from the National Institutes on Deafness and other Communication Disorders (RO1 DC01362 to R. Fettiplace). S. Mahendrasingam was supported by a grant to D.N. Furness from Deafness Research UK.

Edward N. Pugh Jr. served as editor.

Submitted: 23 July 2013
Accepted: 24 September 2013

REFERENCES

Alagramam, K.N., R.J. Goodyear, R. Geng, D.N. Furness, A.F. van Aken, W. Marcotti, C.J. Kros, and G.P. Richardson. 2011. Mutations in protocadherin 15 and cadherin 23 affect tip links and mechanotransduction in mammalian sensory hair cells. *PLoS ONE.* 6:e19183. http://dx.doi.org/10.1371/journal.pone.0019183

Assad, J.A., G.M. Shepherd, and D.P. Corey. 1991. Tip-link integrity and mechanical transduction in vertebrate hair cells. *Neuron.* 7:985–994. http://dx.doi.org/10.1016/0896-6273(91)90343-X

Bats, C., M. Farrant, and S.G. Cull-Candy. 2013. A role of TARPs in the expression and plasticity of calcium-permeable AMPARs: Evidence from cerebellar neurons and glia. *Neuropharmacology.* 74:76–85. http://dx.doi.org/10.1016/j.neuropharm.2013.03.037

Beurg, M., M.G. Evans, C.M. Hackney, and R. Fettiplace. 2006. A large-conductance calcium-selective mechanotransducer channel in mammalian cochlear hair cells. *J. Neurosci.* 26:10992–11000. http://dx.doi.org/10.1523/JNEUROSCI.2188-06.2006

Beurg, M., R. Fettiplace, J.H. Nam, and A.J. Ricci. 2009. Localization of inner hair cell mechanotransducer channels using high-speed calcium imaging. *Nat. Neurosci.* 12:553–558. http://dx.doi.org/10.1038/nn.2295

Chatzigeorgiou, M., S. Bang, S.W. Hwang, and W.R. Schafer. 2013. tmc-1 encodes a sodium-sensitive channel required for salt chemosensation in C. elegans. *Nature.* 494:95–99. http://dx.doi.org/10.1038/nature11845

Coombs, I.D., D. Soto, M. Zonouzi, M. Renzi, C. Shelley, M. Farrant, and S.G. Cull-Candy. 2012. Cornichons modify channel properties of recombinant and glial AMPA receptors. *J. Neurosci.* 32:9796–9804. http://dx.doi.org/10.1523/JNEUROSCI.0345-12.2012

Coste, B., J. Mathur, M. Schmidt, T.J. Earley, S. Ranade, M.J. Petrus, A.E. Dubin, and A. Patapoutian. 2010. Piezo1 and Piezo2 are essential components of distinct mechanically activated cation channels. *Science.* 330:55–60. http://dx.doi.org/10.1126/science.1193270

Coste, B., B. Xiao, J.S. Santos, R. Syeda, J. Grandl, K.S. Spencer, S.E. Kim, M. Schmidt, J. Mathur, A.E. Dubin, et al. 2012. Piezo proteins are pore-forming subunits of mechanically activated channels. *Nature.* 483:176–181. http://dx.doi.org/10.1038/nature10812

Crawford, A.C., M.G. Evans, and R. Fettiplace. 1991. The actions of calcium on the mechano-electrical transducer current of turtle hair cells. *J. Physiol.* 434:369–398.

Dinklo, T., C.J. Meulenberg, and S.M. van Netten. 2007. Frequency-dependent properties of a fluid jet stimulus: calibration, modeling, and application to cochlear hair cell bundles. *J. Assoc.*

Res. Otolaryngol. 8:167–182. http://dx.doi.org/10.1007/s10162-007-0080-0

Fettiplace, R. 2009. Defining features of the hair cell mechanoelectrical transducer channel. *Pflugers Arch.* 458:1115–1123. http://dx.doi.org/10.1007/s00424-009-0683-x

Furness, D.N., and C.M. Hackney. 1985. Cross-links between stereocilia in the guinea pig cochlea. *Hear. Res.* 18:177–188. http://dx.doi.org/10.1016/0378-5955(85)90010-3

Furness, D.N., and C.M. Hackney. 1986. High-resolution scanning-electron microscopy of stereocilia using the osmium-thiocarbohydrazide coating technique. *Hear. Res.* 21:243–249. http://dx.doi.org/10.1016/0378-5955(86)90222-4

Furness, D.N., Y. Katori, B. Nirmal Kumar, and C.M. Hackney. 2008. The dimensions and structural attachments of tip links in mammalian cochlear hair cells and the effects of exposure to different levels of extracellular calcium. *Neuroscience.* 154:10–21. http://dx.doi.org/10.1016/j.neuroscience.2008.02.010

Gale, J.E., W. Marcotti, H.J. Kennedy, C.J. Kros, and G.P. Richardson. 2001. FM1-43 dye behaves as a permeant blocker of the hair-cell mechanotransducer channel. *J. Neurosci.* 21:7013–7025.

Goodyear, R.J., W. Marcotti, C.J. Kros, and G.P. Richardson. 2005. Development and properties of stereociliary link types in hair cells of the mouse cochlea. *J. Comp. Neurol.* 485:75–85. http://dx.doi.org/10.1002/cne.20513

Grati, M., M.E. Schneider, K. Lipkow, E.E. Strehler, R.J. Wenthold, and B. Kachar. 2006. Rapid turnover of stereocilia membrane proteins: evidence from the trafficking and mobility of plasma membrane Ca^{2+}-ATPase 2. *J. Neurosci.* 26:6386–6395. http://dx.doi.org/10.1523/JNEUROSCI.1215-06.2006

Indzhykulian, A.A., R. Stepanyan, A. Nelina, K.J. Spinelli, Z.M. Ahmed, I.A. Belyantseva, T.B. Friedman, P.G. Barr-Gillespie, and G.I. Frolenkov. 2013. Molecular remodeling of tip links underlies mechanosensory regeneration in auditory hair cells. *PLoS Biol.* 11:e1001583. http://dx.doi.org/10.1371/journal.pbio.1001583

Johnson, S.L., M. Beurg, W. Marcotti, and R. Fettiplace. 2011. Prestin-driven cochlear amplification is not limited by the outer hair cell membrane time constant. *Neuron.* 70:1143–1154. http://dx.doi.org/10.1016/j.neuron.2011.04.024

Kawashima, Y., G.S. Géléoc, K. Kurima, V. Labay, A. Lelli, Y. Asai, T. Makishima, D.K. Wu, C.C. Della Santina, J.R. Holt, and A.J. Griffith. 2011. Mechanotransduction in mouse inner ear hair cells requires transmembrane channel-like genes. *J. Clin. Invest.* 121:4796–4809. http://dx.doi.org/10.1172/JCI60405

Kazmierczak, P., H. Sakaguchi, J. Tokita, E.M. Wilson-Kubalek, R.A. Milligan, U. Müller, and B. Kachar. 2007. Cadherin 23 and protocadherin 15 interact to form tip-link filaments in sensory hair cells. *Nature.* 449:87–91. http://dx.doi.org/10.1038/nature06091

Kennedy, H.J., M.G. Evans, A.C. Crawford, and R. Fettiplace. 2003. Fast adaptation of mechanoelectrical transducer channels in mammalian cochlear hair cells. *Nat. Neurosci.* 6:832–836. http://dx.doi.org/10.1038/nn1089

Kim, K.X., and R. Fettiplace. 2013. Developmental changes in the cochlear hair cell mechanotransducer channel and their regulation by transmembrane channel–like proteins. *J. Gen. Physiol.* 141:141–148. http://dx.doi.org/10.1085/jgp.201210913

Kindt, K.S., G. Finch, and T. Nicolson. 2012. Kinocilia mediate mechanosensitivity in developing zebrafish hair cells. *Dev. Cell.* 23:329–341. http://dx.doi.org/10.1016/j.devcel.2012.05.022

Kros, C.J., A. Rüsch, and G.P. Richardson. 1992. Mechano-electrical transducer currents in hair cells of the cultured neonatal mouse cochlea. *Proc. Biol. Sci.* 249:185–193. http://dx.doi.org/10.1098/rspb.1992.0102

Kros, C.J., W. Marcotti, S.M. van Netten, T.J. Self, R.T. Libby, S.D. Brown, G.P. Richardson, and K.P. Steel. 2002. Reduced climbing and increased slipping adaptation in cochlear hair cells of mice with Myo7a mutations. *Nat. Neurosci.* 5:41–47. http://dx.doi.org/10.1038/nn784

Kurima, K., L.M. Peters, Y. Yang, S. Riazuddin, Z.M. Ahmed, S. Naz, D. Arnaud, S. Drury, J. Mo, T. Makishima, et al. 2002. Dominant and recessive deafness caused by mutations of a novel gene, TMC1, required for cochlear hair-cell function. *Nat. Genet.* 30:277–284. http://dx.doi.org/10.1038/ng842

Lazarczyk, M., C. Pons, J.A. Mendoza, P. Cassonnet, Y. Jacob, and M. Favre. 2008. Regulation of cellular zinc balance as a potential mechanism of EVER-mediated protection against pathogenesis by cutaneous oncogenic human papillomaviruses. *J. Exp. Med.* 205:35–42. http://dx.doi.org/10.1084/jem.20071311

Lelli, A., Y. Asai, A. Forge, J.R. Holt, and G.S. Géléoc. 2009. Tonotopic gradient in the developmental acquisition of sensory transduction in outer hair cells of the mouse cochlea. *J. Neurophysiol.* 101:2961–2973. http://dx.doi.org/10.1152/jn.00136.2009

Marcotti, W., S.M. van Netten, and C.J. Kros. 2005. The aminoglycoside antibiotic dihydrostreptomycin rapidly enters mouse outer hair cells through the mechano-electrical transducer channels. *J. Physiol.* 567:505–521. http://dx.doi.org/10.1113/jphysiol.2005.085951

Marcotti, W., A. Erven, S.L. Johnson, K.P. Steel, and C.J. Kros. 2006. Tmc1 is necessary for normal functional maturation and survival of inner and outer hair cells in the mouse cochlea. *J. Physiol.* 574:677–698. http://dx.doi.org/10.1113/jphysiol.2005.095661

Mutai, H., S. Mann, and S. Heller. 2005. Identification of chicken transmembrane channel-like (TMC) genes: expression analysis in the cochlea. *Neuroscience.* 132:1115–1122. http://dx.doi.org/10.1016/j.neuroscience.2005.01.046

Ohmori, H. 1985. Mechano-electrical transduction currents in isolated vestibular hair cells of the chick. *J. Physiol.* 359:189–217.

Pan, B., G.S. Géléoc, Y. Asai, G.C. Horwitz, K. Kurima, K. Ishikawa, Y. Kawashima, A.J. Griffith, and J.R. Holt. 2013. TMC1 and TMC2 are components of the mechanotransduction channel in hair cells of the mammalian inner ear. *Neuron.* 79:504–515. http://dx.doi.org/10.1016/j.neuron.2013.06.019

Partanen, J.I. 2010. Re-evaluation of the thermodynamic activity quantities in aqueous rubidium and cesium chloride solutions at 25°C. *J. Chem. Eng. Data.* 55:249–257. http://dx.doi.org/10.1021/je900320r

Peng, A.W., F.T. Salles, B. Pan, and A.J. Ricci. 2011. Integrating the biophysical and molecular mechanisms of auditory hair cell mechanotransduction. *Nat Commun.* 2:523. http://dx.doi.org/10.1038/ncomms1533

Pickles, J.O., S.D. Comis, and M.P. Osborne. 1984. Cross-links between stereocilia in the guinea pig organ of Corti, and their possible relation to sensory transduction. *Hear. Res.* 15:103–112. http://dx.doi.org/10.1016/0378-5955(84)90041-8

Rard, J.A., and S.L. Clegg. 1997. Critical evaluation of the thermodynamic properties of aqueous calcium chloride. 1. Osmotic and activity coefficients of 0–10.77 mol · kg^{-1} aqueous calcium chloride solutions at 298.15 K and correlation with extended Pitzer ion-interaction models. *J. Chem. Eng. Data.* 42:819–849. http://dx.doi.org/10.1021/je9700582

Ricci, A.J., and R. Fettiplace. 1998. Calcium permeation of the turtle hair cell mechanotransducer channel and its relation to the composition of endolymph. *J. Physiol.* 506:159–173. http://dx.doi.org/10.1111/j.1469-7793.1998.159bx.x

Ricci, A.J., A.C. Crawford, and R. Fettiplace. 2003. Tonotopic variation in the conductance of the hair cell mechanotransducer channel. *Neuron.* 40:983–990. http://dx.doi.org/10.1016/S0896-6273(03)00721-9

Stauffer, E.A., and J.R. Holt. 2007. Sensory transduction and adaptation in inner and outer hair cells of the mouse auditory system.

J. Neurophysiol. 98:3360–3369. http://dx.doi.org/10.1152/jn.00914.2007

Steel, K.P., and G.R. Bock. 1980. The nature of inherited deafness in deafness mice. *Nature.* 288:159–161. http://dx.doi.org/10.1038/288159a0

Vreugde, S., A. Erven, C.J. Kros, W. Marcotti, H. Fuchs, K. Kurima, E.R. Wilcox, T.B. Friedman, A.J. Griffith, R. Balling, et al. 2002. Beethoven, a mouse model for dominant, progressive hearing loss DFNA36. *Nat. Genet.* 30:257–258. http://dx.doi.org/10.1038/ng848

Waguespack, J., F.T. Salles, B. Kachar, and A.J. Ricci. 2007. Stepwise morphological and functional maturation of mechanotransduction in rat outer hair cells. *J. Neurosci.* 27:13890–13902. http://dx.doi.org/10.1523/JNEUROSCI.2159-07.2007

Xiong, W., N. Grillet, H.M. Elledge, T.F. Wagner, B. Zhao, K.R. Johnson, P. Kazmierczak, and U. Müller. 2012. TMHS is an integral component of the mechanotransduction machinery of cochlear hair cells. *Cell.* 151:1283–1295. http://dx.doi.org/10.1016/j.cell.2012.10.041